JOURNAL OF AEROSOL MEDICINE AND PULMONARY DRUG DELIVERY
Volume 29, Number 1, 2016

Pp. 46–56
DOI: 10.1089/jamp.2014.1188

Influence of Mesh Density on Airflow and Particle Deposition in Sinonasal Airway Modeling

Dennis O. Frank-Ito, PhD,[1] Matthew Wofford, MD,[2] Jeffry D. Schroeter, PhD,[3] and Julia S. Kimbell, PhD[2]

Abstract

Background: There are methodological ambiguities in the literature on mesh refinement analysis for computational fluid dynamics (CFD) modeling of physiologically realistic airflow dynamics and particle transport in the human sinonasal cavity. To investigate grid independence in discretization of the (sino)nasal geometry, researchers have considered CFD variables such as pressure drop, velocity profile, wall shear, airflow, and particle deposition fractions. Standardization in nasal geometry is also lacking: unilateral or bilateral nasal cavities with and without paranasal sinuses have been used. These methodological variants have led to inconsistencies in establishing grid-independent mesh densities. The aim of this study is to provide important insight in the role of mesh refinement analysis on airflow and particle deposition in sinonasal airway modeling.
Methods: A three-dimensional reconstruction of the complete sinonasal cavity was created from computed tomography images of a subject who had functional endoscopic sinus surgery. To investigate airflow grid independence, nine different tetrahedral mesh densities were generated. For particle transport mesh refinement analysis, hybrid tetrahedral-prism elements with near-wall prisms ranging from 1 to 6 layers were implemented. Steady-state, laminar inspiratory airflow simulations under physiologic pressure-driven conditions and nebulized particle transport simulations were performed with particle sizes ranging from 1–20 μm.
Results: Mesh independence for sinonasal airflow was achieved with approximately 4 million unstructured tetrahedral elements. The hybrid mesh containing 4 million tetrahedral cells with three prism layers demonstrated asymptotic behavior for sinonasal particle deposition. Inclusion of boundary prism layers reduced deposition fractions relative to tetrahedral-only meshes.
Conclusions: To ensure numerically accurate simulation results, mesh refinement analyses should be performed for both airflow and particle transport simulations. Tetrahedral-only meshes overpredict particle deposition and are less accurate than hybrid tetrahedral-prism meshes.

Key words: airflow, computational fluid dynamics, hybrid mesh, mesh refinement, particle deposition, prism elements, sinonasal cavity, tetrahedral meshes

Introduction

The complexity of the sinonasal cavity lends itself to the creation of anatomically accurate three-dimensional (3D) computational models for simulating physiologically realistic airflow patterns and particle transport using computational fluid dynamics (CFD) techniques. In order to predict aerodynamic behavior accurately, computational simulation conditions such as nasal geometry, mesh density, material properties, and numerical scheme need to be considered. Numerical simulations using the finite element or finite volume methods require very fine meshes to ensure sufficient accuracy of solution results. Since generating fine meshes with good grid quality in the discretization of complex geometries such as the sinonasal cavity can be computationally expensive, the determination of mesh densities sufficient for grid convergence is an important issue in conducting credible CFD simulation studies.

[1]Division of Otolaryngology, Head and Neck Surgery, Duke University Medical Center, Durham, North Carolina.
[2]Department of Otolaryngology, Head and Neck Surgery, University of North Carolina, Chapel Hill, North Carolina.
[3]Applied Research Associates, Inc., Raleigh, North Carolina.

There is a lack of consistency in the literature on the number and type of grid elements required to provide numerically accurate CFD solutions for studies involving sinonasal *in-silico* analysis of airflow and particulate matter,[1–17] even though most investigators performed airflow simulation using the finite volume method software package, Fluent™ (ANSYS, Inc., Canonsburg, PA). Among studies where mesh density analyses were reported, some authors failed to report details regarding how mesh refinement was done to achieve grid-independent numerical solutions.[8–12,18] In situations where particle transport was simulated (Table 1), the mesh structure utilized varied; some authors utilized unstructured tetrahedral meshes,[4–13,19,20] whereas other investigators used a hybrid of tetrahedral and prism meshes.[1–3,14–18,21,22] The inclusion of prism boundary layers increases mesh density near airway walls and is generally considered to provide more accurate near-wall particle trajectory calculations.

Mesh refinement analyses reported in the literature have resulted in a variety of recommended mesh types. This variety is likely due to a combination of the following factors: (1) the complex nature of the nasal anatomy is often confounded by underlying pathology, ethnicity, and natural changes associated with mucosal congestion; as a result, the surface area and volume of the nasal cavity at the time CT or MRI scan was done will vary accordingly. (2) There is lack of standard variables to report during sensitivity analysis. Some researchers reported velocity profile as the basis for conducting mesh refinement,[6,7,16] others reported airflow, deposition fractions, pressure drop, wall shear stress, or combination of CFD variables.[2,3,13,17,20] A number of other investigators did not specify the variables computed to determine grid independent control volume.[1,8–11,14,15] (3) There are no standardized nasal characteristics that investigators conform to when reconstructing nasal geometry for CFD studies. In some articles, CFD analyses were done using unilateral (one side) nasal cavity,[8–11,21,22] while others performed CFD on bilateral (two sides) nasal cavities without the paranasal sinuses[1–3,6,13–15,17–20] or with the paranasal sinuses; as in this study or that of Ge et al.[16]

The present study uses CFD techniques to systematically perform a two-stage mesh sensitivity analysis in an anatomically accurate 3D sinonasal cavity of a subject who underwent functional endoscopic sinus surgery (FESS) as part of treatment for medically recalcitrant chronic rhinosinusitis (CRS). The motivation for using a post-surgery geometry is two-fold: (1) although FESS is not done on the main nasal cavity, successful post-surgery healing restores the patency of the main nasal cavity to that of a normal subject, as was the case in this subject; (2) since the geometry of the sinonasal cavity is more complex than the main nasal cavity, and very little is known about simulating particle transport in post-surgery sinonasal cavity, there is the need to conduct mesh density analysis that produces an accurate total deposition fraction in the sinonasal cavity for post-surgery nebulized drug delivery.

The first stage of our mesh refinement analysis will focus on generating nine different unstructured tetrahedral elements to determine the right density necessary to achieve gird independence based on flow dynamics. Next, we will

Table 1. Volumetric Mesh Density and Type of Nasal Geometric Utilized in the Literature

Year published	*Reference*	*Volume mesh*	*Near-wall mesh*	*Nasal cavity*	*Main outcome of article*
2005	Kleven et al.[4]	Tetra	none	Bilateral	Deposition
2006	Zamankhan et al.[5]	965K and 1.8M tetra	none	Unilateral	Flow and deposition
2006	Inthavong et al.[19]	586K tetra	none	Bilateral	Deposition
2007	Shi et al.[18]	1.7M tetra	4-layer prism	Bilateral	Deposition
2007	Liu et al.[21]	4M tetra	3-layer prism	Unilateral	Deposition
2008	Xi & Longest[3]	1.06M tetra	5-layer pentahedral	Bilateral	Flow and deposition
2008	Inthavong et al.[6]	950K tetra	none	Bilateral	Deposition
2008	Shanley et al.[9]	965K tetra	none	Unilateral	Deposition
2009	Wang et al.[20]	950K tetra	none	Bilateral	Flow and deposition
2010	Chen et al.[7]	2M tetra	none	Bilateral	Deposition
2010	King et al.[13]	1.2M tetra	none	Bilateral	Flow and deposition
2010	Liu et al.[22]	4M tetra	3-layer prism	Unilateral	Deposition
2011	Schroeter et al.[2]	4-9M tetra	3-layer prism	Bilateral	Deposition
2011	Moghadas et al.[11]	600K tetra	none	Unilateral	Deposition
2012	Frank et al.[14]	4 M tetra	3-layer prism	Bilateral	Deposition
2012	Frank et al.[1]	4 M tetra	3-layer prism	Bilateral	Deposition
2012	Abouali et al.[10]	3.5M tetra	none	Unilateral	Deposition
2012	Chen et al.[8]	2.45M tetra	none	Unilateral	Deposition
2012	Ghalati et al.[12]	2.6M tetra	none	Bilateral (with trachea)	Flow and deposition
2012	Ge et al.[16]	4M tetra	6-layer prism	Bilateral (with sinuses)	Flow and deposition
2012	Li et al.[17]	3.5M tetra	prism layer	Bilateral	Flow and deposition
2013	Frank et al.[15]	4 M tetra	3-layer prism	Bilateral	Deposition

K, thousand; M, million; and tetra, tetrahedral.

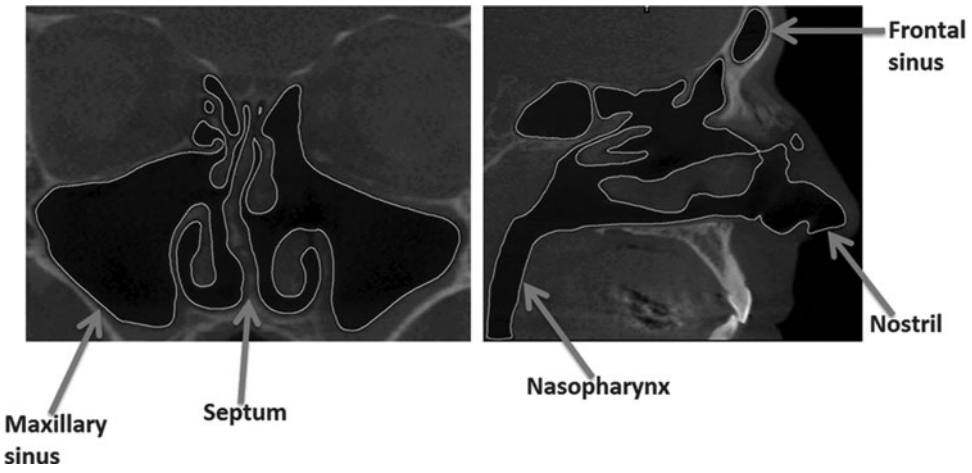

FIG. 1. Sinonasal cavity of the subject after functional endoscopic sinus surgery. *Left panel*: Coronal view; *right panel*: Sagittal view.

create different prism configurations to investigate the effect of adding prism layers on particle deposition calculations, as well as assessing for prism parameters that achieve mesh independence for nasal particle transport in the nose.

Methods

Nasal model reconstruction

A 39-year-old Caucasian male subject (94.5 kg) who underwent FESS for the treatment of medically recalcitrant CRS (Fig. 1) was recruited for this study. Written informed consent was provided as required by the Institutional Review Board at the University of North Carolina at Chapel Hill. A medical imaging software, Mimics™ 14.01 (Materialise, Inc., Plymouth, MI) was used to create a 3D reconstruction of the nasal and paranasal cavities from the subject's post-FESS computed tomography (CT) scans. The CT protocol generated 270 slices, with an increment of 0.399 mm, and a pixel size of 0.4 mm. Surface area and volume of the subject's 3D reconstructed post-FESS sinonasal passage were approximately 35,978 mm^2 and 86,019 mm^3, respectively. The 3D sinonasal model was imported into the mesh generation software package ICEM-CFD™ 12.1 (ANSYS, Inc., Canonsburg, PA) in stereolithography (STL) file format. Planar nostril and outlet surfaces, as well as the main nasal cavity and maxillary sinuses regions for tracking particle deposition were created.

Mesh refinement

Mesh refinement analysis was conducted in two stages. The first stage focused on the tetrahedral mesh forming the basis of the CFD model. Grid convergence was investigated for variables that were sensitive to nasal airway mesh density. These variables included volumetric airflow rate for a fixed pressure drop, transnasal pressure drop, and airflow velocity profiles. The second stage of analysis focused on mesh structure near airway walls. Grid convergence was investigated for variables affected by high near-wall gradients. These variables involved

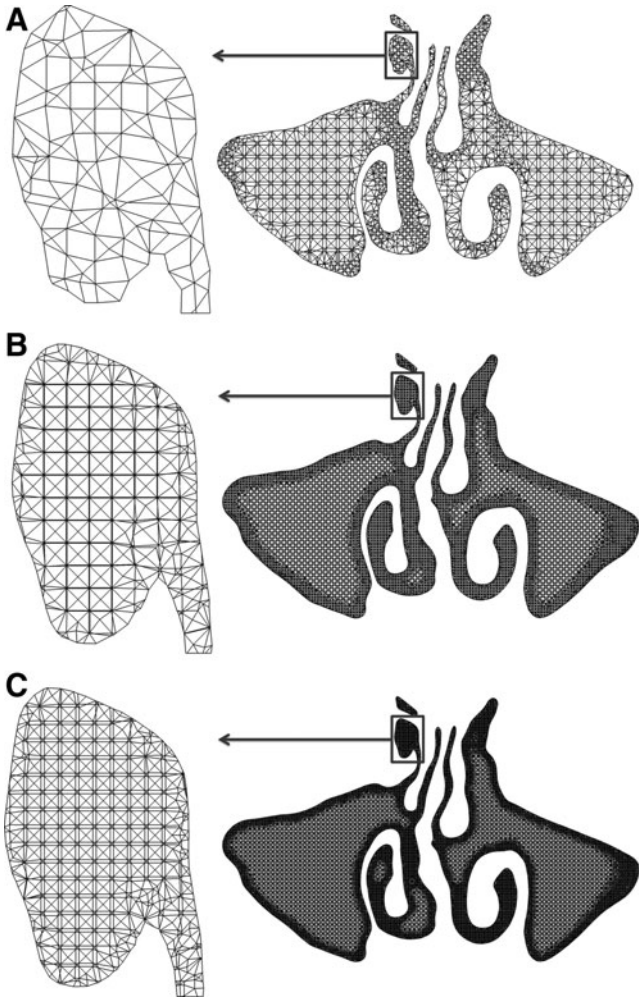

FIG. 2. Unstructured tetrahedral elements: **(A)** 0.25 million cells, **(B)** 4 million cells, and **(C)** 8 million cells.

particle transport simulation and included overall and regional deposition fractions.

First-stage mesh refinement: Airflow simulation. Nine different global mesh densities of unstructured tetrahedral elements were generated (Fig. 2), consisting of 0.25, 0.5, 1, 2, 3, 4, 5, 6, and 8 million cells with a maximum element size of 1, and tetrahedral size ratio of 1.1 to induce grading when possible toward airway walls. These grid densities were made by varying the mesh global element scale factor in ICEM-CFD™ accordingly to achieve the desired number of grid elements. Mesh quality analysis was performed to minimize effects of distorted elements on the accuracy of the numerical flow simulation (tetrahedral element aspect ratio required to be >0.3). To determine the effects of mesh density on simulated airflow, the following CFD variables were reported (Fig. 3): volume flow rate at the outlet (L/min), pressure drop from nostrils to posterior end of the septum (Pa), anterior-to-posterior air velocity magnitude profile across the right side maxillary sinus antrostomy (surgically-created opening from the main nasal cavity into the maxillary sinus), and lateral-to-medial air velocity magnitude profile across the left airspace at the posterior end of septum (m/s).

Second-stage mesh refinement: Particle transport. Particle transport mesh refinement analysis based on total sinonasal deposition was conducted (Fig. 4) by constructing prism layers near the airway wall using the smallest unstructured tetrahedral grid that provided mesh independent numerical airflow results above. This was done systematically by varying: (a) total prism zone thickness; (b) size of each prism layer; and (c) number of prism layers. Sensitivity analysis for simulated particle transport in the sinonasal cavity was conducted in two steps: (1) fix the size of each individual prism layer to be 0.1 mm and vary total prism zone thickness from 0.1 to 0.4 mm (1 to 4 layers); and (2) based on the outcome in step (1), fix the total prism zone thickness and divide into 1 to 6 layers, which varied the thickness of the individual prism layers. Mesh quality analysis was performed to minimize distortion from skewed elements (element quality required to be greater than >0.1).

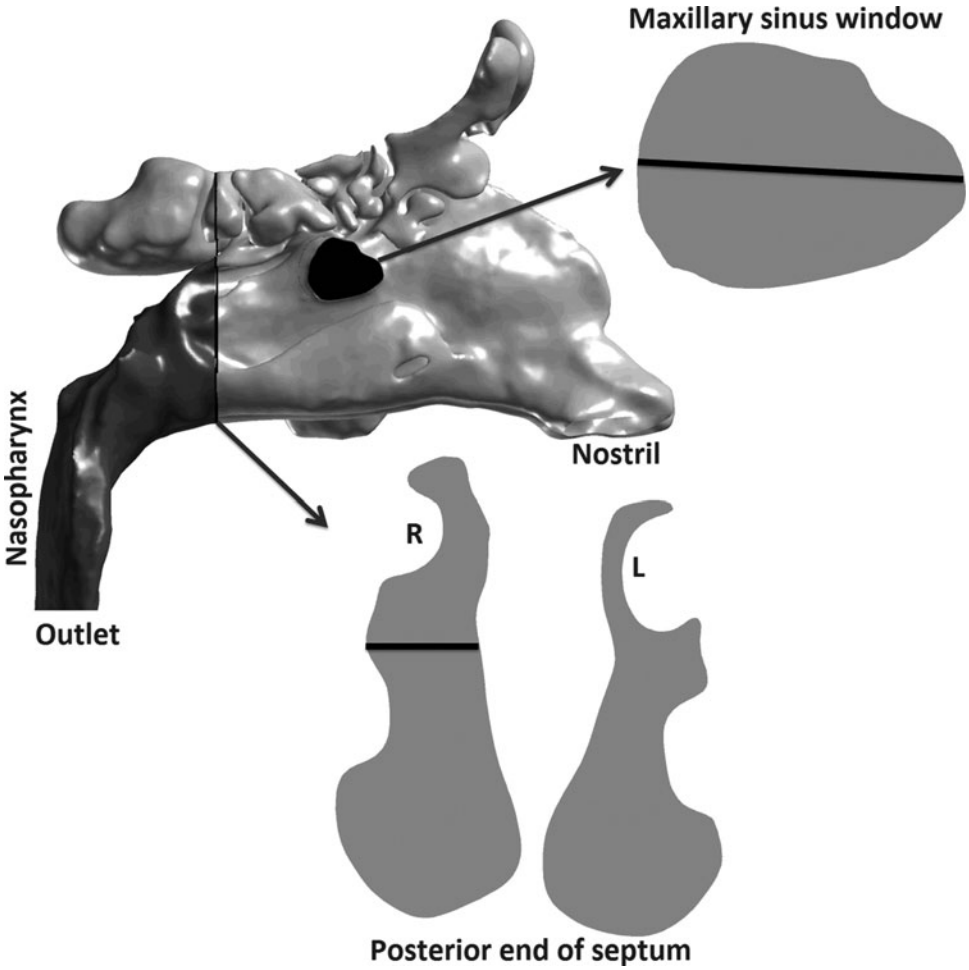

FIG. 3. Locations of sinonasal airway where CFD variables were reported for fluid flow mesh sensitivity analysis. Velocity magnitudes were calculated at the *solid black lines* along the *right side* maxillary sinus window and the *cross-sectional* posterior end of the septum, volume flow rate at the outlet, and transnasal pressure drop from nostrils to the posterior end of the septum

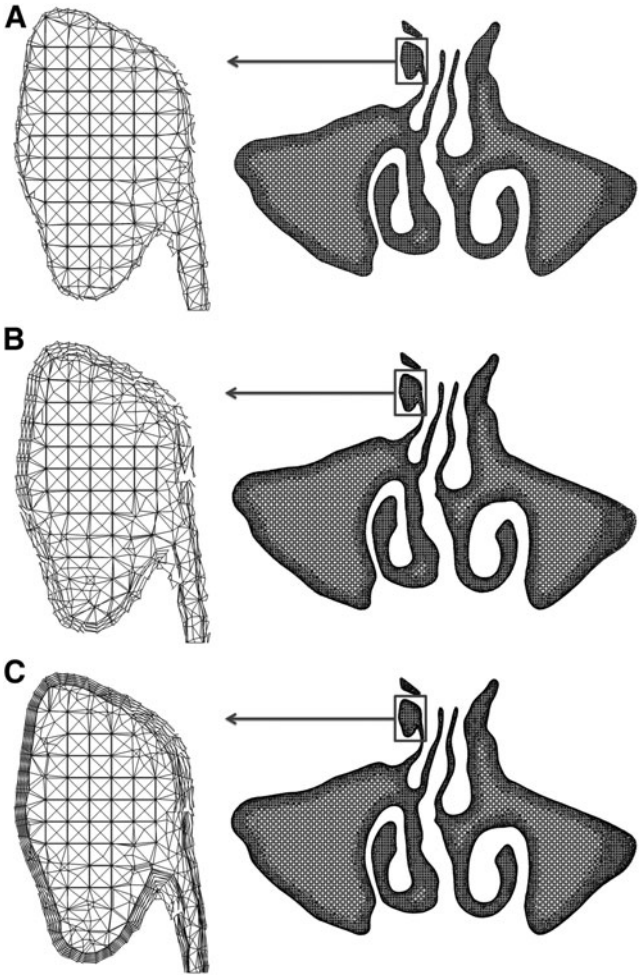

FIG. 4. Hybrid tetrahedral-prism mesh elements, prism layers were created from an existing 4 million unstructured tetrahedral cells: **(A)** one prism layer with prism thickness of 0.1 mm, **(B)** three prism layers with total prism thickness of 0.3 mm, and **(C)** six prism layers with total prism thickness of 0.3 mm.

CFD simulation. Uncoupled numerical simulations of airflow and particle transport were conducted in this study. Steady-state, laminar inspiratory airflow was simulated using Fluent™ 12.1.4 under physiologic pressure-driven conditions. Although sinonasal airflow can sometimes become turbulent at higher flow rates occurring during sniffing or exercise, there is evidence that laminar conditions dominate nasal airflow at resting to moderate breathing rates of ≤ 25 L/min.[3,9,23] Simulation at steady-state assumes that time-dependent variables were constant and all derivatives with respect to time were zero. Fluent uses the finite volume method to numerically solve the Navier-Stokes equations. The conservation of mass and momentum for laminar incompressible flow are described, respectively, by the equations

$$\nabla \cdot \vec{u} = 0,$$

$$\rho(\vec{u} \cdot \nabla)\vec{u} = -\nabla p + \mu \nabla^2 \vec{u},$$

where $\vec{u} = \vec{u}(x, y, z)$ is the velocity vector, ρ is the fluid density, μ is dynamic viscosity, and p is pressure. In this study, $\rho = 1.204\,\text{kg/m}^3$ and $\mu = 1.825 \times 10^{-5}\,\text{kg/m-s}$. The boundary conditions specified in the airflow simulations were:[1,14,15,24,25]

- A ''wall'' condition, assuming that the walls were stationary with zero air velocity at the air-wall interface.
- A ''pressure-inlet'' condition at the nostrils with gauge pressure set to zero.
- A ''pressure-outlet'' condition at the outlet with gauge pressure set to -10.36 Pascal.

The next phase of the simulations dealt with simulating particle trajectories in the sinonasal cavity to predict total sinonasal deposition. The setup for this simulation mimics nebulized aerosol delivery with inspiratory airflow present. Particles were released evenly across the nostril surface to mimic nebulized drug delivery, with particle size distribution set to range in aerodynamic diameter from 1–20 μm (1 μm increments and about 20,000 particles per size). Particle trajectories were calculated using the Discrete Phase Model in Fluent, assuming spherical particles of unit density under the Lagrangian equations of motion for particles, given by

$$\frac{du_p}{dt} = F_D(u - u_p) + \frac{g(\rho_p - \rho)}{\rho_p}$$

where $F_D(u - u_p)$ is the drag force per unit particle mass. And

$$F_D = \frac{18\mu}{\rho_p d_p^2}\frac{C_D Re}{24},$$

where u is the fluid phase velocity, u_p is the particle velocity, μ is the molecular viscosity of the fluid, ρ is the fluid density, ρ_p is the density of the particle, d_p is the particle diameter, C_D is the drag coefficient. The relative Reynolds number, Re is defined as

$$Re = \frac{\rho d_p |u_p - u|}{\mu}.$$

For $\rho = 1.204\,\text{kg/m}^3$, $\rho_p = 1000\,\text{kg/m}^3$, $d_p = 1\text{-}20\,\mu$m, and $u_p = 0$ m/s. Sinonasal particle deposition fractions (SPDF) were expressed as

$$SPDF = \frac{Number\ of\ deposited\ particle\ in\ the\ sinonasal\ cavity}{Number\ of\ particles\ released}$$

Localized particle deposition fractions were computed in the following regions: left and right sides of the nasal vestibule; left and right sides of the middle nasal cavity (anterior inferior turbinates to choanae); left and right maxillary sinuses; and nasopharynx.

Results

Airflow simulation

Plots displaying outlet volume flow rate versus mesh density (Fig. 5a), and pressure drop from nostrils to posterior end of septum versus mesh density (Fig. 5b) showed that asymptotic behavior of outlet volume flow rate and transnasal pressure drop began to occur around 4 million

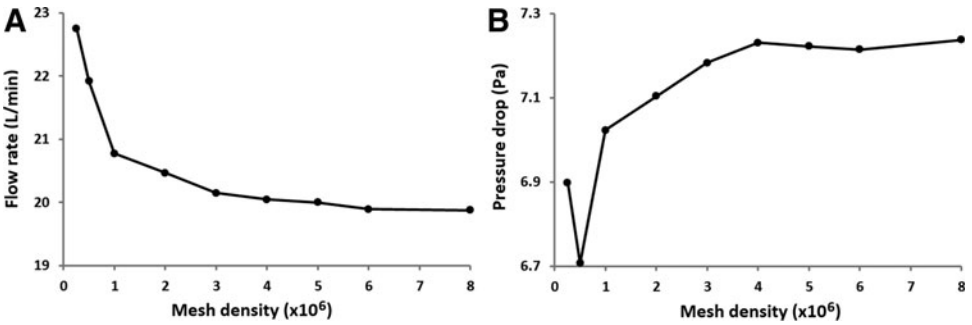

FIG. 5. Computed CFD variables for nine different unstructured tetrahedral cells: **(A)** Volume flow rate (L/min) at the outlet, and **(B)** transnasal pressure drop from nostril to posterior end of septum.

tetrahedral mesh elements, indicating mesh density insensitivity in these variables beyond 4 million cells: The relative changes (between 4 and 5 million mesh elements) in outlet flow rate and transnasal pressure drop were within 0.2% and 0.1%, respectively. Velocity magnitude line plots are reported in Figure 6 for right maxillary sinus window and cross-sectional posterior end of septum. Convergence of velocity magnitude at the posterior end of septum was not clearly achieved at any of the simulated mesh density (Fig. 6a); nonetheless, asymptotic behavior of velocity magnitude on the right maxillary sinus window was observed at 1 million tetrahedral elements (Fig. 6b).

Particle transport simulation

Fine-layer prism elements were created near the walls of the sinonasal cavity from the 4 million, tetrahedral-cell meshes. Simulation predictions of particle deposition with the size of each prism layer set at 0.1 mm showed collapsed total sinonasal deposition fractions for hybrid tetrahedral-prism meshes of two-layer, three-layer, and four-layer prism cells (Fig. 7a). Asymptotic particle deposition behavior appears more pronounced at three-layer prism elements with total prism thickness of 0.3 mm. Higher deposition fractions were predicted for both one-layer prism cells (hybrid) and 4 million tetrahedral cells without prisms (Fig. 7a). Next, by fixing total prism thickness at 0.3 mm, sinonasal particle deposition fractions showed similar deposition (Fig. 7b) for the following hybrid tetrahedral-prism meshes: two-layer with size of each layer = 0.15 mm; three-layer with size of each layer = 0.1 mm; four-layer with size of each layer = 0.075 mm; and six-layer with size of each layer = 0.05 mm. Higher deposition fractions were recorded for one-prism layer with size of each layer = 0.3 mm and 4 million tetrahedral cells without prism elements (Fig. 7b).

To investigate the effects of near-wall prism cells on sinonasal deposition, nebulized particle deposition fractions for different tetrahedral mesh densities (4, 6, and 8 million) and hybrid tetrahedral-prism elements (three-layer with size of each prism layer = 0.1 mm were created on existing 4, 6, and 8 million tetrahedral elements) were compared. Simulation results (Fig. 7c) showed that meshes with tetrahedral elements alone predicted higher sinonasal particle deposition than their corresponding hybrid prism-tetrahedral meshes. Increasing mesh density beyond the converged control volume had little impact on deposition behavior for the hybrid mesh structures, but increasing tetrahedral-only mesh density further decreased SPDF.

Regional deposition fractions in the left and right maxillary sinuses are displayed in Figure 8. Particle deposition patterns into the left maxillary sinus were very sensitive to mesh density for both varying prism layers and thickness (Fig. 8A), and varying prism layers for a fixed thickness of 0.3 mm (Fig. 8B). On the contrary, changes in particle deposition patterns in the right maxillary sinus appeared to have less variation to mesh density (Fig. 8C and 8D). Simulated particle transport results demonstrated a much stronger evidence of grid convergence at the hybrid 4

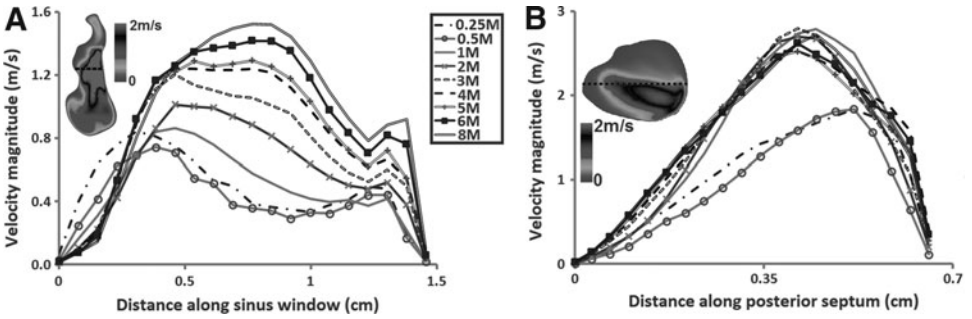

FIG. 6. Computed velocity magnitude for nine different unstructured tetrahedral cells: **(A)** Along the cross-sectional posterior end of septum, and **(B)** along the maxillary sinus window.

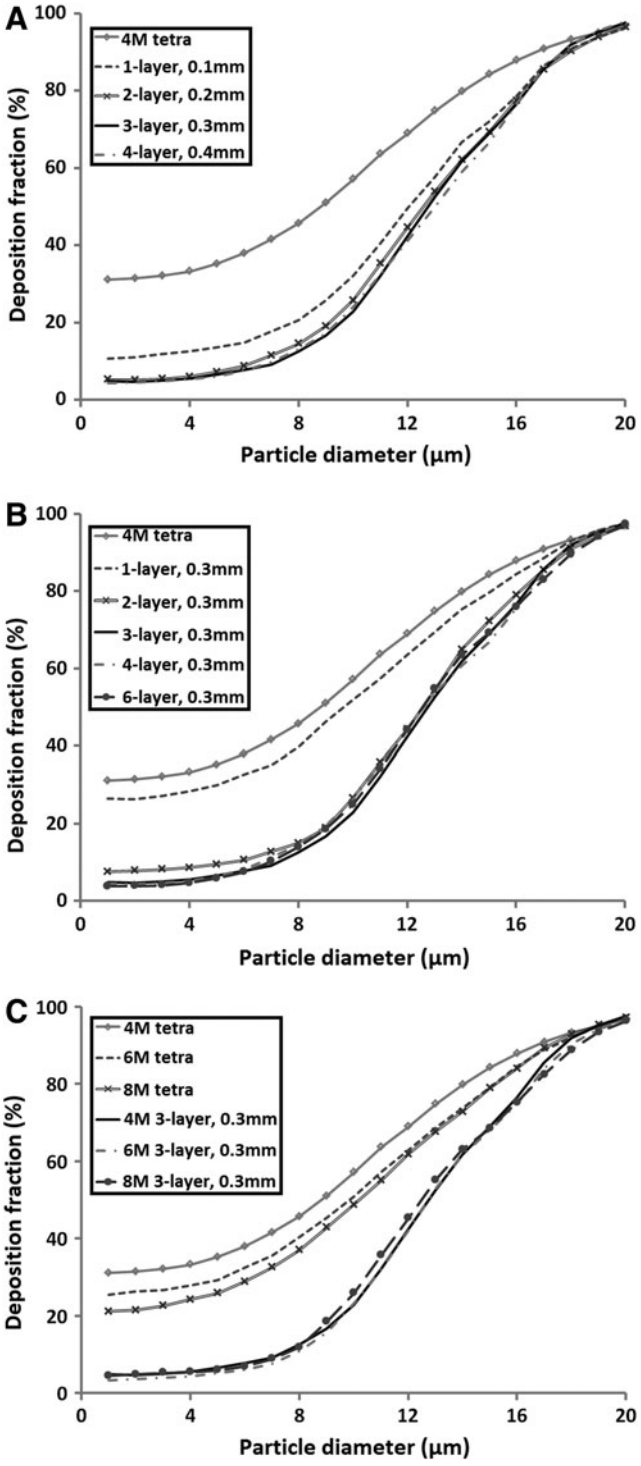

FIG. 7. Total sinonasal deposition fraction mesh characteristics: **(A)** Comparing varying prism layers and thickness with 4 million tetrahedral only cells, **(B)** comparing varying prism layers for a fixed thickness of 0.3 mm with 4 million tetrahedral only cells, and **(C)** comparing 4 million, 6 million, and 8 million tetrahedral only elements with their corresponding hybrid tetrahedral-prism meshes.

million tetrahedral elements with three-prismatic layers and total thickness of 0.3 mm in Figure 8D (plots comparing varying prism layers for a fixed thickness of 0.3 mm) than in Figure 8C.

Figure 9 shows regional depositions along the main nasal cavity comparing 1 to 6 prism layers for a fixed thickness of 0.3mm in the hybrid mesh elements. Convergence of local deposition at the nasal vestibule was much stronger on the right side than on the contralateral side (Fig. 9A and 9B). Particle deposition behavior in the middle nasal cavity and nasopharynx regions were slightly more sensitive to mesh density than in the nasal vestibule. In addition, simulated results showed less variability to number of prism layers at smaller particle sizes (less than 10 microns) than at larger particle sizes (10–20 microns) in both middle nasal cavity and nasopharynx regions (Fig. 9C–9E).

In Figure 10, we further assessed the importance of two-staged mesh refinement (tetrahedral and prism) versus one-staged refinement (tetrahedral) on particle deposition by comparing nasal deposition fractions from experimental data in Kelly et al.[26] with simulated results from tetrahedral-only 4 million elements and hybrid tetrahedral-prism mesh density of 4 million tetrahedral elements with three-prism layers of 0.3 mm (size of each layer was 0.1 mm). Curve fitting plots of deposition fractions as a function of deposition parameter ($DP = d_p^2 \Delta P$, where Q is inhaled flow rate and ΔP is transnasal pressure drop from the nostrils to the end of the septum)[27] revealed a consistently good agreement between the hybrid tetrahedral-prism mesh with experimental data at every particle size range; but was not the case for the 4 million tetrahedral-only mesh.

Discussion

Airflow mesh refinement sensitivity analysis performed in this study on the entire (left and right passages) sinonasal cavity revealed asymptotic behavior around 4 million unstructured tetrahedral elements with relative change in outlet volume flow rate within 0.2%, and 0.1% for transnasal pressure drop. Mesh density analysis on typical sinonasal geometries similar to that used in this article have reported grid convergence at varying densities. Inthavong and colleagues[19] achieved mesh independence based on airflow velocity profile in a human nasal passage at 586,000 tetrahedral elements; and 950,000 cells in subsequent articles by this group.[6,20] Grid convergence analysis performed by other investigators have reported anywhere between 1.2 and 2.45 million tetrahedral cells are required to ensure numerically independent results.[7,8,13] Grid refinement analysis done by King and colleagues[13] converged at 1.2 million cells since velocity profiles exhibited $< 0.5\%$ change when mesh density was increased to 2.6 million cells. In agreement with the findings in the present report, Ge and colleagues[16] achieved mesh density convergence based on outlet velocity profiles around 4 million cells.

Mesh convergence analysis in the literature on particle transport in the (sino)nasal passage did not report details about near wall prism refinement in many cases.[1-3,14–18,21,22] Approximately 4–5 million elements were needed in the refinement analysis done by Schroeter et al.[2] to ensure that airflow and particle trajectory results were independent of

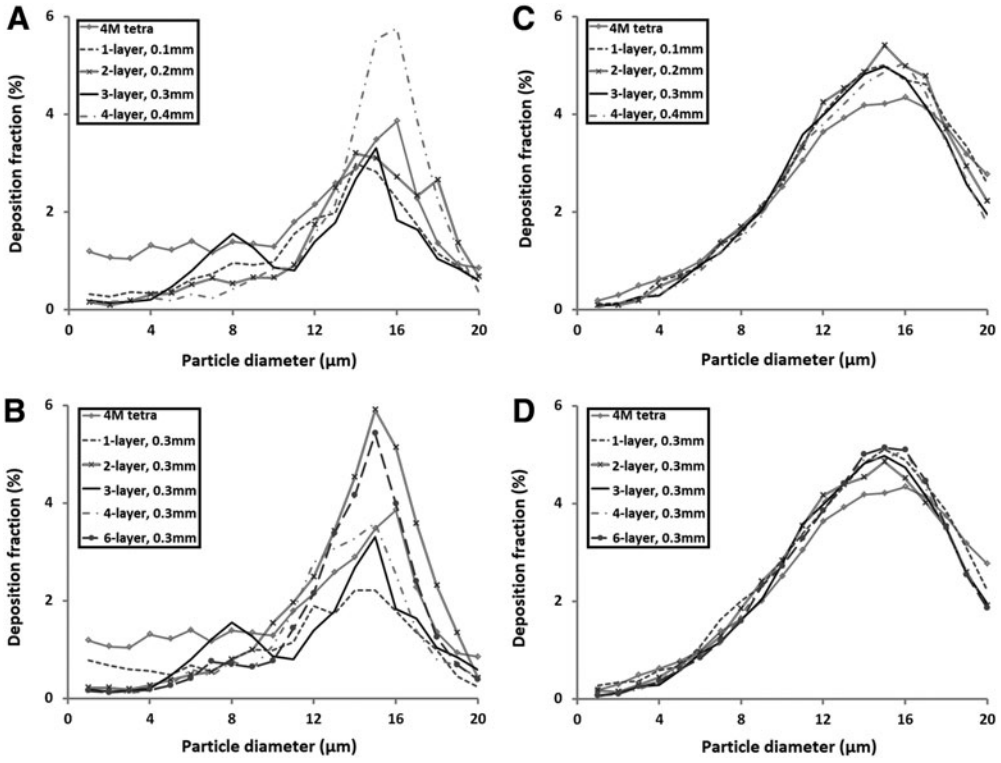

FIG. 8. Regional deposition fraction in the maxillary sinuses: **(A)** Deposition into the left maxillary sinus comparing varying prism layers and thickness with 4 million tetrahedral only cells, **(B)** deposition into the left maxillary sinus comparing varying prism layers for a fixed thickness of 0.3 mm with 4 million tetrahedral only cells, **(C)** deposition into the right maxillary sinus comparing varying prism layers and thickness with 4 million tetrahedral only cells, and **(D)** deposition into the right maxillary sinus comparing varying prism layers for a fixed thickness of 0.3 mm with 4 million tetrahedral only cells.

mesh density in their smoothed models; near wall prism refinement was not conducted. Grid sensitivity analysis performed by Xi and Longest[3] evaluated four different mesh densities with a five-layer pentahedral elements, but no information was provided on how the choice of five layers was determined. Similarly, Liu and colleagues[21,22] used three prism layers in their work, but did not discuss analysis of prism configuration during mesh refinement. Shi et al.[18] reported that enhanced numerical accuracy was achieved with a refined near wall mesh density of prism layers; yet did not report how they decided on a four-layer prism boundary of 0.2 mm total thickness. Both Ge et al.[16] and Li et al.[17] did not specify the kind of prism-layer refinement analysis done in their respective studies.

Interestingly, although the 3D geometries in the present study and in Kelly et al.[26] were quite different, nasal deposition fractions from our hybrid tetrahedral-prism mesh aligned nicely with experimental data. Our geometry included the sinuses and is a post-surgery sinonasal anatomy with obvious anatomic changes from surgery, while the geometry in Kelly et al.[26] was from a normal subject and did not include the sinuses. These differences did not influence deposition results in our hybrid tetrahedral-prism mesh model using the deposition parameter (DP) equation. In addition, while there may be no real justification for a comparison of results from an abnormal sinonasal cavity with a normal nasal cavity, the experimental data help inform us that our simulation results are converging to the correct solution as the mesh is refined. Nonetheless, it is worth noting that plotting nasal deposition fractions against DP has been used by other authors to account for interindividual variability;[27,28] and CFD studies have shown that for deposition comparisons in similar geometries with that of Kelly et al.[26] a much stronger relationship was observed when deposition fractions were plotted against DP, rather than the impaction parameter ($IP = d_p^2 Q$).[2, 12]

Particle deposition results in the present study revealed that prism mesh independence was robust at three-prism layers with size of each layer set at 0.1 mm (resulting in a total prism thickness of 0.3 mm). However, it should be noted that predicted local deposition patterns in the left maxillary sinus did not demonstrate convergence of deposition results around a particular mesh density; the right maxillary sinus had less sensitive deposition fractions to mesh density. Simulated localized deposition patterns along the anterior posterior region of the main nasal cavity showed better convergence at the nasal vestibule compared to the middle nasal cavity and nasopharynx regions. In general, these results suggest that certain regions of the sinonasal cavity may benefit from additional local mesh control and refinement in order to achieve localized grid independence.

We note that generalizations cannot be made from our findings to support the notion that 4 million unstructured

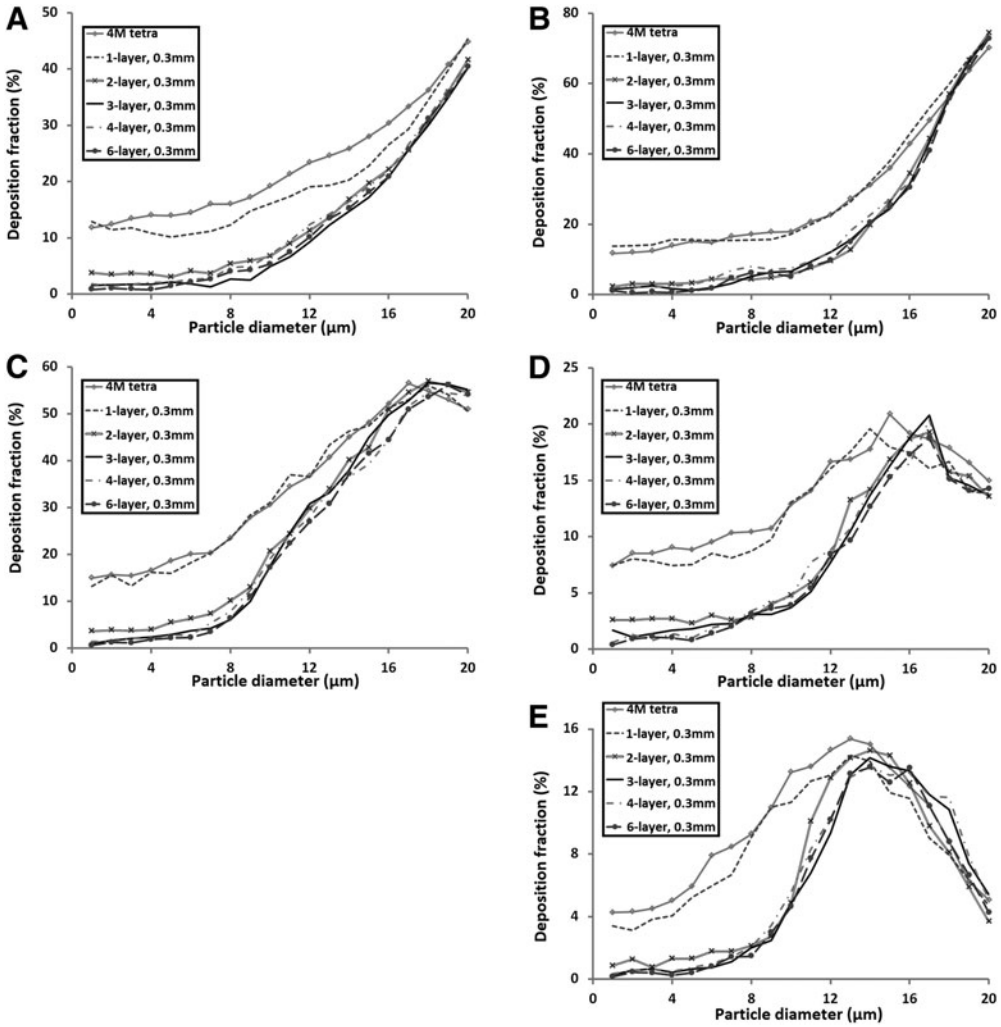

FIG. 9. Regional deposition fraction comparing varying (1–6) prism layers for a fixed thickness of 0.3 mm with 4 million tetrahedral only cells: **(A)** Left nasal vestibule, **(B)** Right nasal vestibule, **(C)** Left middle nasal cavity, **(D)** Right middle nasal cavity, and **(E)** Naso-pharynx.

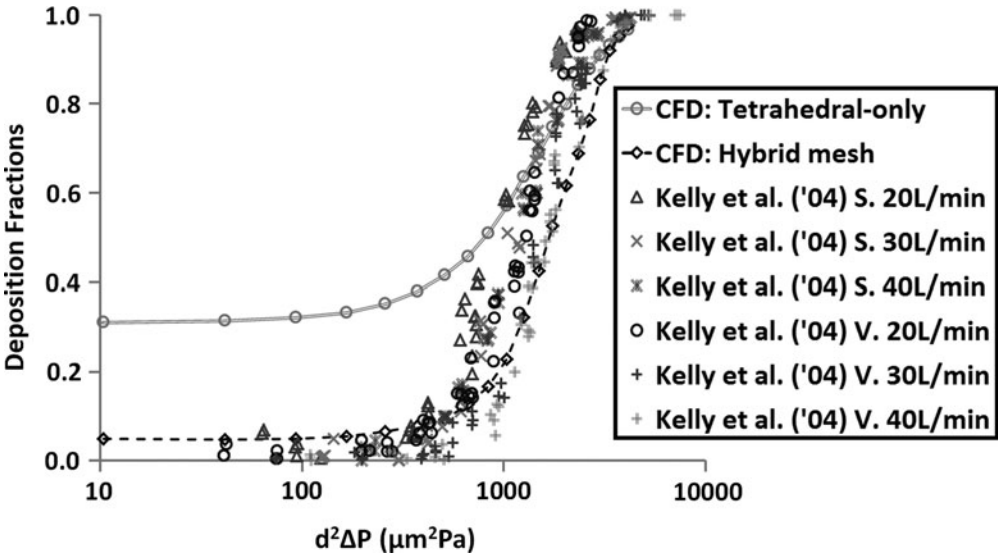

FIG. 10. Comparison of CFD predicted deposition fractions as a function of deposition parameter with experimental data from Kelly et al.[26] for their SLA (S) and Viper (V) nasal replica models.

tetrahedral elements with near-wall three-prism layers is the only mesh structure that yield accurate flow and particle transport predictions. In fact, other mesh types, such as hexahedra used by Kimbell and colleagues,[29] as well as any structured mesh type, can also produce accurate flow and particle transport predictions; rather this study emphasizes the importance of mesh refinement for attaining trustworthy computational solutions. In addition, mesh-independent density required to accurately capture turbulent-particle interactions for modeling turbulence may not necessary be the same density for laminar flow since the fluid flow regime between turbulence and laminar behavior differently. For example, simulating the transport of particles into the nose during rapid breathing (sniffing) or a combination of different rapid breathing frequencies and amplitudes via solving the unsteady equations governing turbulent fluid flow to explicitly resolve time-dependent eddies will likely require some form of adaptive mesh refinement, unlike the scenario presented in the present study.

A number of different factors can influence deposition of particulate matter in the sinonasal airway, for example, the presence of nasal anatomic deformities have been shown to compromise the airway morphology (size and share), which in turn greatly impact deposition behavior.[1,14,15] Similarly, wall roughness has been determined to influence particle deposition, with reported higher deposition efficiencies in nasal models with rough walls compared to models with smoothed walls.[2,12,18,20] The effects of wall roughness on mesh density analysis in a given nasal model with varying degree of wall roughness are poorly understood. Although it can be inferred from the present study that once mesh-independent density is achieved, consistent total deposition pattern may be attained across nasal geometries of different morphologies and wall roughness since that was the case in our comparison with Kelly et al.,[26] where deposition curves collapsed when plotted as a function of deposition parameter, further studies need to be done to investigate to the role of nasal morphology and wall roughness on mesh refinement analysis.

In conclusion, a finite-volume mesh density sensitivity analysis study on the sinonasal airway of a FESS subject who had surgery for the treatment of refractory chronic rhinosinusitis was conducted to illustrate the importance of mesh refinement on sinonasal flow and particle transport. Nine different unstructured tetrahedral elements between 0.25 million and 8 million cells were generated in the sinonasal geometry; CFD-derived airflow variables were calculated for each density. Hybrid tetrahedral-prism meshes of varying prism layers and thicknesses were created to analyze grid-independent particle deposition results. Our findings are threefold: first, grid convergence pertaining to sinonasal airflow was observed around 4 million unstructured tetrahedral mesh density; second, the inclusion of boundary prism layers substantially reduces deposition behavior relative to purely tetrahedral meshes; third, the hybrid tetrahedral-prism mesh density of 4 million tetrahedral cells with three-layer prism elements (total prism thickness of 0.3 mm) demonstrated asymptotic behavior for sinonasal particle deposition. CFD results presented in this study confirm that mesh density can influence flow dynamics and aerosolized particle deposition in the sinonasal cavity.

Acknowledgment

We would like to acknowledge Drs. Adam M. Zanation, Charles S. Ebert, Jr., Brent A. Senior, Gitanjali M. Fleischman, and Kibwei A. McKinney for recruitment, treatment of the subject, and general clinical advice.

Author Disclosure Statement

Research reported in this article was supported by the National Institute on Deaftness and Other Communication Disorders of the National Institutes of Health under Award Number T32DC005360. The content is solely the responsibility of the authors and does not necessarily represent the official views of the National Institutes of Health.

References

1. Frank DO, Kimbell JS, Pawar S, and Rhee JS: Effects of anatomy and particle size on nasal sprays and nebulizers. Otolaryngol Head Neck Surg. 2012;146:313–319.
2. Schroeter JD, Garcia GJ, and Kimbell JS: Effects of surface smoothness on inertial particle deposition in human nasal models. J Aerosol Sci. 2011;42:52–63.
3. Xi J, and Longest PW: Numerical predictions of submicrometer aerosol deposition in the nasal cavity using a novel drift flux approach. Intl J Heat Mass Transfer. 2008; 51:5562–5577.
4. Kleven M, Melaaen MC, Reimers M, Røtnes JS, Aurdal L, and Djupesland PG: Using computational fluid dynamics (CFD) to improve the bi-directional nasal drug delivery concept. Food Bioproducts Process. 2005;83:107–117.
5. Zamankhan P, Ahmadi G, Wang Z, Hopke PK, Cheng YS, Su WC, and Leonard D: Airflow and deposition of nanoparticles in a human nasal cavity. Aerosol Sci Technol. 2006; 40:463–476.
6. Inthavong K, Tian ZF, Tu JY, Yang W, and Xue C: Optimising nasal spray parameters for efficient drug delivery using computational fluid dynamics. Comp Biol Med. 2008; 38:713–726.
7. Chen XB, Lee HP, Chong VF, and Wang de Y: A computational fluid dynamics model for drug delivery in a nasal cavity with inferior turbinate hypertrophy. J Aerosol Med Pulm Drug Deliv. 2010;23:329–338.
8. Chen XB, Lee HP, Chong VF, and Wang DY: Drug delivery in the nasal cavity after functional endoscopic sinus surgery: A computational fluid dynamics study. J Laryngol Otol. 2012;126:487–494.
9. Shanley KT, Zamankhan P, Ahmadi G, Hopke PK, and Cheng YS: Numerical simulations investigating the regional and overall deposition efficiency of the human nasal cavity. Inhal Toxicol. 2008;20:1093–1100.
10. Abouali O, Keshavarzian E, Farhadi Ghalati P, Faramarzi A, Ahmadi G, and Bagheri MH: Micro and nanoparticle deposition in human nasal passage pre and post virtual maxillary sinus endoscopic surgery. Respir Physiol Neurobiol. 2012;181:335–345.
11. Moghadas H, Abouali O, Faramarzi A, and Ahmadi G: Numerical investigation of septal deviation effect on deposition of nano/microparticles in human nasal passage. Respir Physiol Neurobiol. 2011;177:9–18.
12. Ghalati PF, Keshavarzian E, Abouali O, Faramarzi A, Tu J, and Shakibafard A: Numerical analysis of micro- and nanoparticle deposition in a realistic human upper airway. Comput Biol Med. 2012;42:39–49.

13. King S, Mei C, Inthavong K, and Tu J: Inhalability of micron particles through the nose and mouth. Inhal Toxicol. 2010;22:287–300.
14. Frank DO, Kimbell JS, Cannon D, Pawar SS, and Rhee JS: Deviated nasal septum hinders intranasal sprays: A computer simulation study. Rhinology. 2012;50:311–318.
15. Frank DO, Kimbell JS, Cannon D, and Rhee JS: Computed intranasal spray penetration: Comparisons before and after nasal surgery. Intl Forum Allergy Rhinol. 2013;3:48–55.
16. Ge QJ, Inthavong K, and Tu JY: Local deposition fractions of ultrafine particles in a human nasal-sinus cavity CFD model. Inhal Toxicol. 2012;24:492–505.
17. Li X, Inthavong K, and Tu J: Particle inhalation and deposition in a human nasal cavity from the external surrounding environment. Build Environ. 2012;47:32–39.
18. Shi H, Kleinstreuer C, and Zhang Z: Modeling of inertial particle transport and deposition in human nasal cavities with wall roughness. Aerosol Sci. 2007;38:398–419.
19. Inthavong K, Tian ZF, Li HF, Tu JY, Yang W, Xue CL, and Li CG: A numerical study of spray particle deposition in a human nasal cavity. Aerosol Sci Technol. 2006;40:1034–1045.
20. Wang SM, Inthavong K, Wen J, Tu JY, and Xue CL: Comparison of micron- and nanoparticle deposition patterns in a realistic human nasal cavity. Respir Physiol Neurobiol 2009;166:142–151.
21. Liu Y, Matida EA, Gu J, and Johnson MR: Numerical simulation of aerosol deposition in a 3-D human nasal cavity using RANS, RANS/EIM, and LES. J Aerosol Sci. 2007;38:683–700.
22. Liu Y, Matida EA, and Johnson MR: Experimental measurements and computational modeling of aerosol deposition in the Carleton-Civic standardized human nasal cavity. J Aerosol Sci. 2010;41:569–586.
23. Kelly JT, Prasad AK, and Wexler AS: Detailed flow patterns in the nasal cavity. J Appl Physiol. 2000;89:323–337.
24. Rhee JS, Pawar SS, Garcia GJ, and Kimbell JS: Toward personalized nasal surgery using computational fluid dynamics. Arch Facial Plast Surg 2011;13:305–310.
25. Kimbell JS, Garcia GJ, Frank DO, Cannon DE, Pawar SS, and Rhee JS: Computed nasal resistance compared with patient-reported symptoms in surgically treated nasal airway passages: A preliminary report. Am J Rhinol Allergy. 2012;26:94–98.
26. Kelly JT, Asgharian B, Kimbell JS, and Wong BA: Particle deposition in human nasal airway replicas manufactured by different methods. Part I: Inertial regime particles. Aerosol Sci Technol. 2004;38:1063–1071.
27. Hounam RF, Black A, and Walsh M: The deposition of aerosol particles in the nasopharyngeal region of the human respiratory tract. Aerosol Sci. 1971;2:47–61.
28. Garcia GJ, Tewksbury EW, Wong BA, and Kimbell JS: Interindividual variability in nasal filtration as a function of nasal cavity geometry. J Aerosol Med Pulm Drug Deliv. 2009;22:139–155.
29. Kimbell JS, Segal RA, Asgharian B, Wong BA, Schroeter JD, Southall JP, Dickens CJ, Brace G, and Miller FJ: Characterization of deposition from nasal spray devices using a computational fluid dynamics model of the human nasal passages. J Aerosol Med. 2007;20:59–74.

Received on October 10, 2014
in final form, March 14, 2015

Reviewed by:
Chantal Darquenne
Ira Katz

Address correspondence to:
Dennis O. Frank-Ito, PhD
Division of Otolaryngology–Head and Neck Surgery
Duke University Medical Center
Box 3805
Durham, NC 27710

E-mail: dennis.frank@duke.edu